# Leaky-Wave Analysis of Transient Fields Due to Sources in Planarly Layered Media

George W. Hanson, *Senior Member, IEEE,* Alexander B. Yakovlev, *Senior Member, IEEE,* and Jin Hao

***Abstract*—The transient field due to canonical sources in planarly layered media is obtained using a leaky-wave analysis. By proper choice of integration paths in both the complex frequency and complex wavenumber planes, transient fields are obtained exactly as a temporal inversion integral over a discrete sum of residues. The residues include both proper and improper surface-wave modes, analytically continued into the complex frequency plane. The method is applicable for all times of interest, although for certain source-receiver locations an "early-time" period is identified which encompasses the specular reflection from the nearest interface, and during which time the residue series requires special treatment. The presented analysis leads to a computationally simple and efficient method for obtaining transient fields due to sources in layered media. Results are shown for the transient potential due to line and point sources over a grounded dielectric slab, although the technique is applicable to multiple planar layers.**

***Index Terms*—Electromagnetic transient analysis, electromagnetic transient propagation, nonhomogeneous media, surface waves.**

## I. Introduction

TRANSIENT analysis of fields due to nonharmonic sources is a classic area of electromagnetic theory, and is regaining importance in light of the current emphasis on ultrawideband radars and high clock-rate digital processors, among other applications. In this paper, we present an efficient and physically insightful leaky-wave analysis of the transient radiation from line and point sources embedded in layered media.

There are basically two classes of techniques for solving transient electromagnetics problems. One method involves solving Maxwell's equations directly in the time-domain, either in differential (e.g., finite-difference time-domain) or integral (e.g., time-domain integral equation) form. Another general technique is to solve Maxwell's equations in the frequency domain and perform an inverse Fourier transform to recover the time-domain fields. Regarding the latter method, a large number of papers have appeared involving layered-media geometries. In [1] and [2], a double deformation technique was applied to the problem of line and point sources in dispersive layered media. This method consists of a steepest descent evaluation of both the spatial-wavenumber and temporal-frequency inversion integrals associated with the time-domain solution. In [3]–[5], a method was developed to treat sources in dispersive layered media, with the spatial inversion performed subsequent to the temporal inversion, leading to the concept of time-domain leaky modes. In [6], an explicit inversion technique based on the Cagniard-de-Hoop method was applied to a line-source in a lossless two-media configuration. The case of a line source in a lossy two-media configuration was analyzed in [7] using a semi-numerical implementation of the Cagniard integration contour. A recent paper [8] considered a multilayer lossless environment using a seminumerical Cagniard-de-Hoop method. In [9], some closed-form expressions were obtained for a point source over an anisotropic lossless interface. In [10] and [11], exact image theory was used for the analysis of dipoles in the presence of a lossless dielectric interface. Many other relevant works may be found in the references of these papers.

In this paper, we expand on a method developed in the geophysical literature [12]–[15] and subsequently applied to the electromagnetic TE line-source problem [16]. The method involves evaluating the spatial-wavenumber inversion integral using complex-plane analysis, resulting in a frequency-domain field in the form of a discrete residue series and a continuous branch-cut integral. Upon deformation of the temporal-frequency plane inversion contour and inclusion of improper modes in the residue series, the transient branch-cut integral contribution is shown to vanish (for certain times). The resulting time-domain field is obtained as a temporal inversion of the residue series, which leads to rapidly convergent, one-dimensional integrals. Although the analytical details required to develop the method are involved, the result is simple, physically insightful, and easy to implement on a computer. The method leads to an efficient computation of the transient field due to a source in a layered medium and is applicable to multilayered, lossy media, although numerical results are only presented for the case of a grounded dielectric slab.

This paper begins with a summary of the properties of surface-waves on a grounded dielectric slab when frequency is continued into the complex plane, followed by the leaky-wave analysis. Since the direct source-to-receiver contribution may be calculated in closed form, the method is applied to all other wave-field contributions, which physically represent waves reflected from the various interfaces, and may include lateral wave contributions.

An important contribution of this paper is to clarify the "early-time" and "late-time" interpretation of the residue series. The analysis presented in [12]–[15] is developed for all time $t > \tau$, where $\tau$ represents the least travel-time of the first arriving wavefield component. In these papers, which consider multiple dielectric layers, the source and observation points are always in different layers. In [16], the problem of a TE line-source over a

Manuscript received February 26, 2002; revised January 17, 2002.

G. W. Hanson and J. Hao are with the Department of Electrical Engineering, University of Wisconsin, Milwaukee, WI 53211 USA.

A. B. Yakovlev is with the Department of Electrical Engineering, The University of Mississippi, University, MS 38677 USA.

Digital Object Identifier 10.1109/TAP.2003.809100

grounded dielectric slab is considered using this method, where the direct contribution is found analytically and the contribution from the dielectric slab is obtained using leaky-waves. However, in this case (source and observation point in the same layer) it is shown here that two distinct time intervals must be considered, called early-time and late-time. The residue series is only applicable during late-time, and its application during early-time, which includes the specular reflection from the nearest interface, leads to erroneous numerical results. This was confirmed by comparison to the numerical results from a fullwave method. For this reason, the numerical results in [16] for this early-time period are incorrect. It is shown here that a simple modification of the residue terms allow for an accurate calculation of the early-time response as well, and with this modification, the transient fields may be calculated as a modified residue series for all $t > \tau$.

## II. Formulation

### A. Complex Frequency-Plane Singularities of Background Waveguide

Knowledge of the complex frequency-plane singularities associated with the discrete surface-wave modes of a laterally infinite, planarly layered structure is important in understanding the leaky-wave analysis to follow. For simplicity, we consider the modes associated with a single grounded lossless slab, although the analysis is similar for any number of planar layers, excepting the single interface case which may be treated analytically. Although the complex frequency plane forms an infinitely sheeted surface for the discrete surface-wave modes, in the following the terms proper and improper sheet exclusively refer to the two-sheeted Riemann surface in the propagation wavenumber $(\lambda)$ plane.

For the structure depicted in Fig. 1, $\mathrm{TM}^z$-even and $\mathrm{TE}^z$-odd modes may propagate, governed by the dispersion equations

$$\begin{aligned} Z^{\mathrm{TE}}(\lambda,\omega) =& m_{21}^2 p_1 + p_2 \coth(p_2 d) \\ =& 0 \\ Z^{\mathrm{TM}}(\lambda,\omega) =& n_{21}^2 p_1 + p_2 \tanh(p_2 d) \\ =& 0 \end{aligned} \tag{1}$$

where $p_i = \sqrt{\lambda^2 - k_i^2}$, $\lambda^2 = k_x^2 + k_z^2$, $k_i^2 = m_i^2 n_i^2 (\omega/c)^2$, and $c = (\mu_0 \varepsilon_0)^{-1/2}$, with $m_i, n_i$ being the magnetic and electric indices of refraction, respectively, $i = 1, 2$, and where $n_{21} = (n_2/n_1)$, and $m_{21} = (m_2/m_1)$. Note that here $\lambda$ is a radial wavenumber and not wavelength.

The factor $p_1$ induces branch points in the complex $\lambda$-plane at $\lambda = \pm k_1$. Proper (above cutoff) modes reside on the proper Riemann sheet where $\mathrm{Re}(p_1) > 0$ (wave dependence is of the form $e^{-p_1 y}$), and improper (below cutoff) modes reside on the improper Riemann sheet where $\mathrm{Re}(p_1) < 0$. The branch cuts which separate these two sheets are defined by

$$\mathrm{Re}(p_1) = 0$$

leading to the standard hyperbolic branch cuts [17]

$$\begin{aligned} \mathrm{Im}(\lambda) =& \frac{\mathrm{Im}(k_1)\,\mathrm{Re}(k_1)}{\mathrm{Re}(\lambda)} \\ |\mathrm{Re}(\lambda)| <& |\mathrm{Re}(k_1)|. \end{aligned} \tag{2}$$

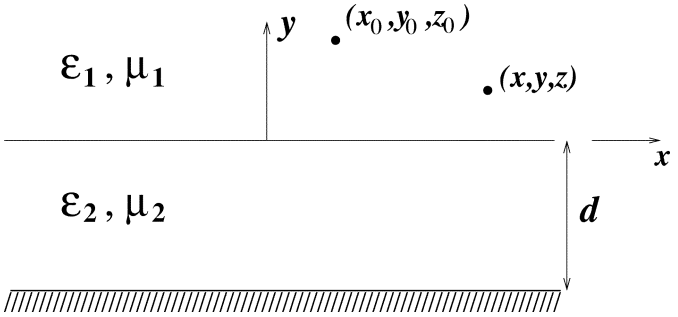


Fig. 1. Electromagnetic source located at $(x_0, y_0, z_0)$ and observation point $(x, y, z)$ in the vicinity of a grounded material layer.

The usual procedure to obtain surface-wave modes is to set a frequency value $\omega$ and search for the value of radial wavenumber $\lambda = \lambda_n(\omega)$ such that $Z(\lambda_n, \omega) = 0$. This leads to the implicitly defined dispersion function $\lambda_n^{(\pm)}(\omega)$, which provides the dispersion behavior for the $n$th mode on the proper $(+)$ or improper $(-)$ Riemann sheet. In this paper, $n = 0, 2, 4, \ldots$ for $\mathrm{TM}^z$-even modes and $n = 1, 3, 5, \ldots$ for $\mathrm{TE}^z$-odd modes.

For illustrative purposes to explain the pole dynamics, in this section we consider the $\mathrm{TM}^z$-even modes of a lossless slab. A detailed analysis of the complex frequency-plane singularities for these modes is given in [18] and references therein; however, for completeness a summary will be provided here. To be consistent with [18], in this section modes associated with a grounded slab (Fig. 1) of thickness $d = 1$ cm characterized by $\varepsilon_1 = \varepsilon_0$, $\varepsilon_2 = 2.25\varepsilon_0$, and $\mu_1 = \mu_2 = \mu_0$ will be described. The various singularities and special points in the right-half complex frequency plane for the $\mathrm{TM}^z$-even modes are shown in Fig. 2. Although Fig. 2 is quite complicated, an understanding of this figure completely explains all possible modal interactions as frequency is varied in the complex plane.

We first consider the case $\omega = 0$. An infinite set of discrete improper modes $\lambda_n^{(-)}(0)$ exist. Actually, corresponding to each different $n$ four different propagation constants [roots of (1)] can be found symmetrically in the four quadrants of the complex $\lambda$-plane $\lambda_{n,i}^{(-)}(0)$, $i = 1, 2, 3, 4$, where $i$ indicates the $\lambda$-plane quadrant number. The roots in the four quadrants are related as $\lambda_{n,4}^{(-)}(0) = \overline{\lambda}_{n,1}^{(-)}(0)$ (the overbar indicates complex conjugate), $\lambda_{n,2}^{(-)}(0) = -\lambda_{n,4}^{(-)}(0)$, and $\lambda_{n,3}^{(-)}(0) = -\lambda_{n,1}^{(-)}(0)$. Their locations are given by the four combinations

$$\lambda_n^{(-)}(0) = \pm\frac{1}{2d}\ln\left(\frac{n_{21}^2+1}{n_{21}^2-1}\right) \pm \frac{j\pi(n-1)}{2d} \tag{3}$$

for $n = 2, 4, 6, \ldots$, where in (3) and in the sequel, we dispense with the double-index notation for simplicity. For $n = 0$ (i.e., the $\mathrm{TM}_0$ mode, which has no low-frequency cutoff), $\lambda_0^{(+)}(0) = 0$. The configuration of modes for $\omega = 0$ is depicted in Fig. 3 of [18]. In the following, we will call a mode and its (initial, i.e., for $\omega = 0$) conjugate a mode pair, designated as $\left(\lambda_n(\omega), \tilde{\lambda}_n(\omega)\right)$, i.e., modes originating in the first and fourth quadrants for $\omega = 0$ form one mode pair, and modes in the second and third quadrants form another mode pair. Note that the conjugate symmetry observed in (3) is generally lost when $\omega \neq 0$.

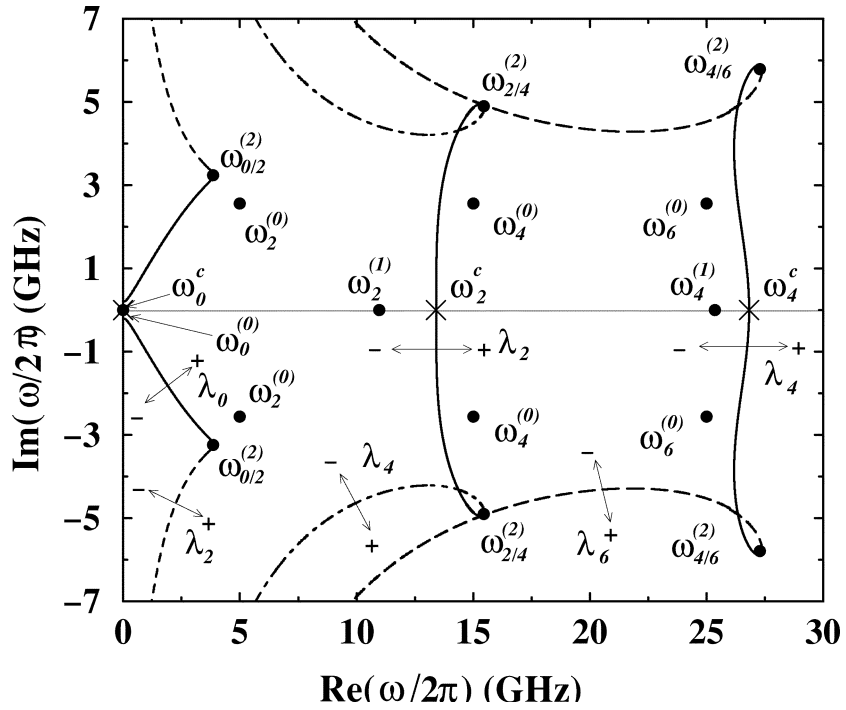


Fig. 2. Complex frequency-plane singularities (dots), generalized cutoff-frequency loci (solid and dashed lines), and ordinary cutoff frequencies (crosses) for the $\mathrm{TM}^z$-even modes of the grounded slab waveguide shown in Fig. 1; $\varepsilon_1 = \varepsilon_0$, $\varepsilon_2 = 2.25\varepsilon_0$, and $d = 1$ cm.

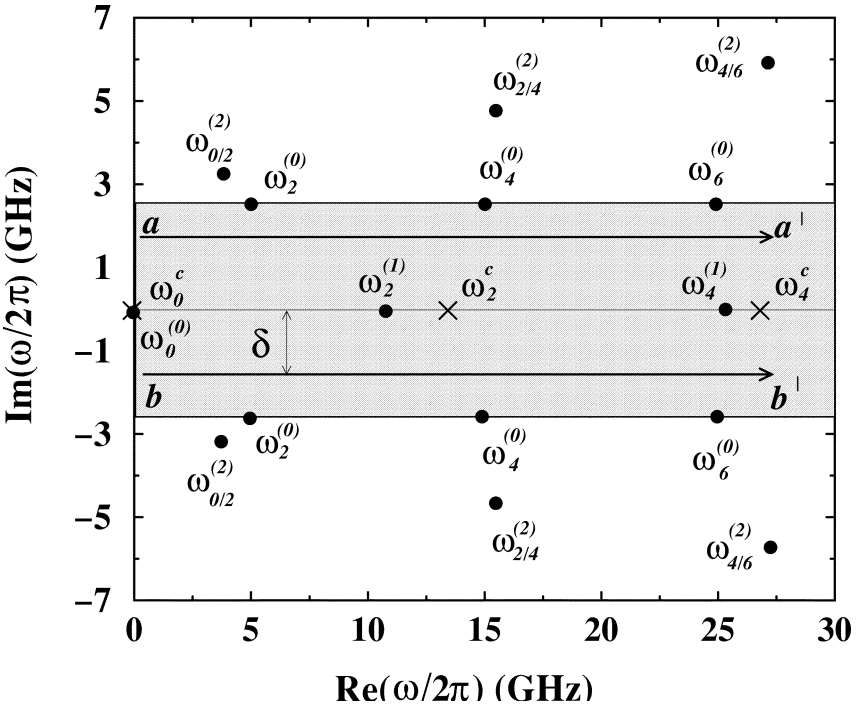


Fig. 3. Complex frequency plane showing two paths for frequency variation ($a - a'$ and $b - b'$). The trajectories of the $\mathrm{TM}_2^z$ modes $\lambda_2$ when frequency varies over these paths are shown in Figs. 4 and 5, and the shaded region indicates the strip where Fourier inversion is performed.

As frequency is increased from $\omega = 0$ along the positive real $\omega$ axis shown in Fig. 2, $\lambda_0^{(+)}(\omega)$ moves away from the origin along the real-$\lambda$ axis, always staying on the proper sheet. Each of the modes in a mode pair $\left(\lambda_n^{(-)}(\omega), \tilde{\lambda}_n^{(-)}(\omega)\right)$ for $n > 0$ follow a trajectory maintaining conjugate symmetry until the point, $\omega_n^{(1)}$ is reached. At this point the modes in the pair meet on the real $\lambda$ axis, temporarily forming a second-order root of (1). Between $\omega_n^{(1)}$ and $\omega_n^c$ (the cutoff frequency) the modes in the pair move in different directions along the real-$\lambda$ axis. The mode which moves away from the origin remains on the improper Riemann sheet for all real frequencies $\omega > \omega_n^{(1)}$. The other mode, which initially moves toward the origin along the real-$\lambda$ axis, passes through the $\lambda$-plane branch point $\lambda = \pm k_1$ when $\omega = \omega_n^c$ and moves onto the proper $\lambda$-plane Riemann sheet.

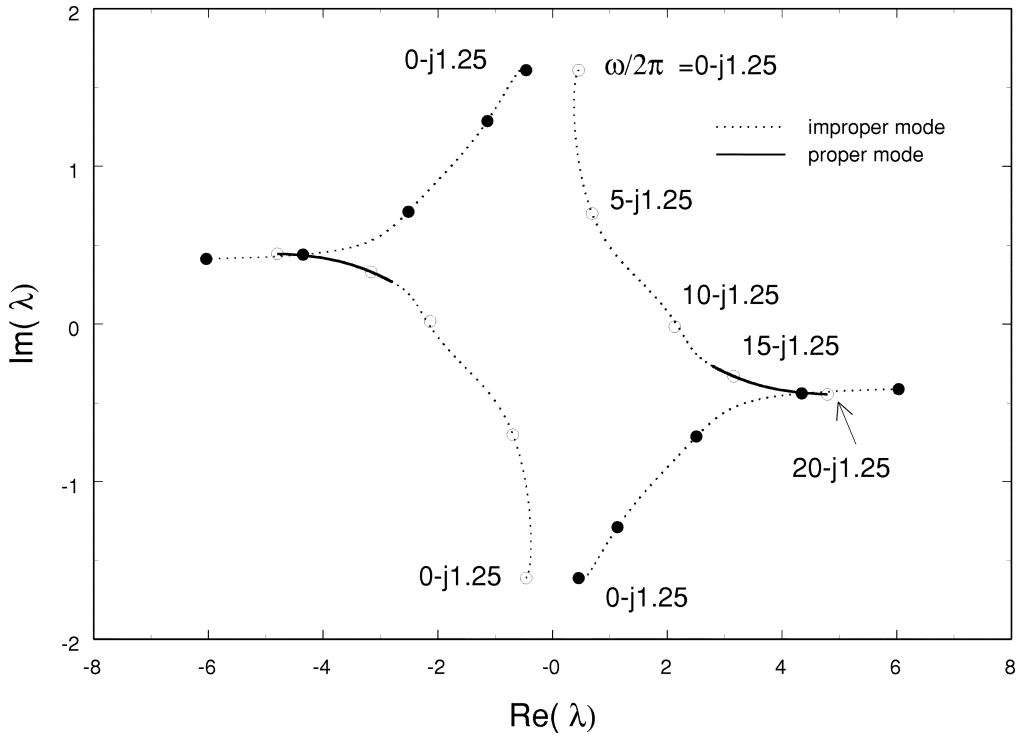


Fig. 4. Trajectory of $\pm(\lambda_2, \bar{\lambda}_2)$ modes in the complex $\lambda$-plane parameterized by real frequency, as frequency is varied along the path $b - b'$ shown in Fig. 3, with $\mathrm{Im}(\omega/2\pi) = 1.25$ GHz. The first circle indicates $\omega/2\pi = 0 - j1.25$ GHz, and subsequent circles indicate frequency progression along the path $b - b'$. Since the frequency path passes below the branch point $\omega_2^{(1)}$ the modes originating in the first and third quadrants of the $\lambda$-plane pass onto the proper Riemann sheet upon crossing the generalized cutoff loci at $\omega/2\pi = 13.43 - j1.25$ GHz.

As frequency further increases, that mode (the usual proper surface-wave mode) moves along the real-$\lambda$ axis away from the origin, becoming asymptotic to $\pm k_2$ for large frequency. This dispersion behavior is shown in [18, Fig. 4].

In the $\omega$-plane the points $\omega_n^{(1)}$ (which may be called the leaky-mode cutoff frequency since below this frequency one obtains the traditional leaky modes) are branch points for the mode pair $\left(\lambda_n(\omega), \tilde{\lambda}_n(\omega)\right)$, although the cutoff frequencies $\omega_n^c$ are not branch points. The $\omega_n^{(1)}$ branch points are located on the real-$\omega$ axis for lossless media, near to and at a value less than the well-known cutoff frequency points

$$\omega_n^c = \frac{n\pi c}{2d\sqrt{m_2^2 n_2^2 - m_1^2 n_1^2}}$$

$n = 0, 2, 4, \ldots$, and can be found numerically from [18] and [19]

$$Z\left(\lambda_n^{(-)}, \omega_n^{(1)}\right) = Z'_\lambda\left(\lambda_n^{(-)}, \omega_n^{(1)}\right) = 0 \tag{4}$$

subject to the nonzero condition

$$Z'_\omega\left(\lambda_n^{(-)}, \omega_n^{(1)}\right) Z''_{\lambda\lambda}\left(\lambda_n^{(-)}, \omega_n^{(1)}\right) \neq 0 \tag{5}$$

where $Z = Z^{\mathrm{TM}}$. It was pointed out in [19] that (4) and (5) are sufficient conditions to guarantee $\omega_n^{(1)}$ is a branch point.

When one allows frequency to be complex, in this case to perform transient analysis, many interesting features emerge. First, we discuss the concept of generalized cutoff frequencies, originally introduced in [18].

The usual definition of modal cutoff in open boundary waveguides is obtained by considering the real-valued frequency $\omega_n^c$ at which an improper mode moves through a $\lambda$-plane branch point to become a proper mode (residing on the proper $\lambda$-plane sheet), as described earlier. Of course, it is not necessary for a mode to pass through the $\lambda$-plane branch point to move between $\lambda$-plane Riemann sheets. Any frequency path that causes the mode to cross the hyperbolic $\lambda$-plane branch cuts (2) will result in a transition between improper and proper $\lambda$-plane Riemann sheets. Complex frequencies at which the mode crosses the $\lambda$-plane branch cut are called generalized cutoff frequencies (in the case of real $\omega$ this reduces to the usual definition of cutoff frequency). These generalized cutoff frequencies will satisfy (1), along with the additional condition $\mathrm{Re}(p_1) = 0$. Unfortunately, this does not lead to an explicit formula for the locus of generalized cutoff frequencies, but rather yields three real equations in three real unknowns ($\omega_r$, $\omega_i$, and $\lambda_r$ or $\lambda_i$). The generalized cutoff loci for several low-order $\mathrm{TM}^z$ modes were determined numerically for the slab under consideration and are shown in Fig. 2. The solid lines (passing through the ordinary cutoff points $\omega_n^c$) represent the locus of frequencies at which one of the modes from the $n$th mode pair (indicated by the double-headed arrow in the figure) crosses the $\lambda$-plane branch cuts. The other mode of the pair remains on the improper sheet. Note that this notion of a generalized cutoff loci is not unique in that other $\lambda$-plane branch cuts will result in other generalized cutoff frequency loci, all passing through $\omega_n^c$ for the $n$th mode. The choice shown here, consistent with the usual hyperbolic $\lambda$-plane branch cuts, is perhaps the most physically meaningful.

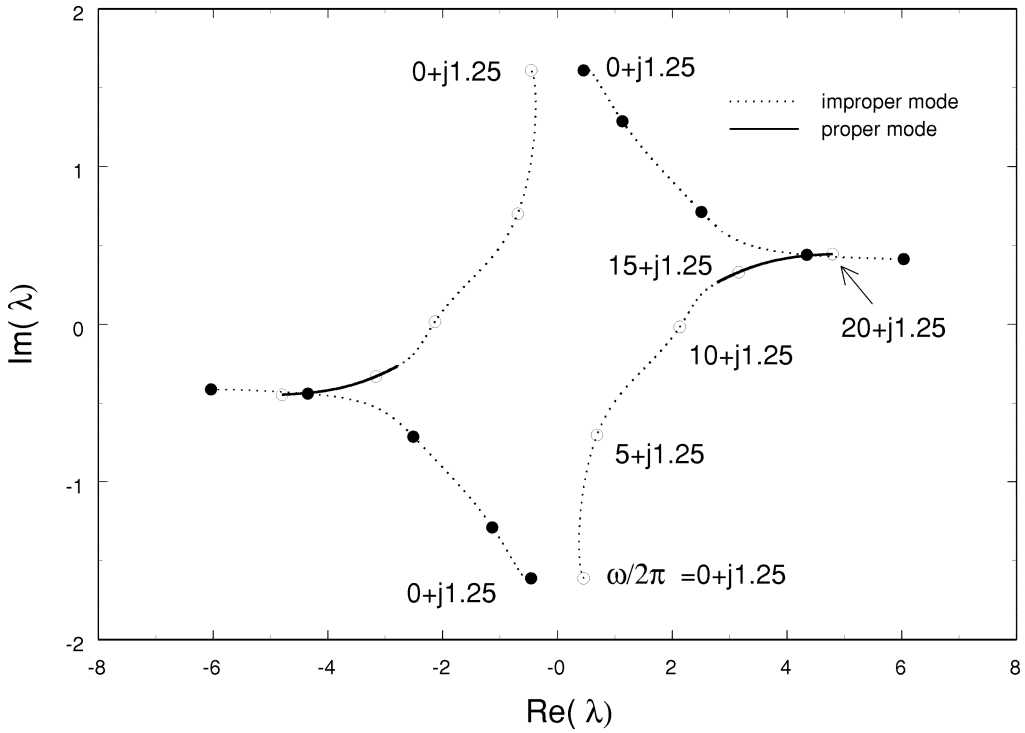


Fig. 5. Similar to Fig. 4, although frequency is varied along the path $a - a'$ shown in Fig. 3. Since the frequency path passes above the branch point $\omega_2^{(1)}$ the modes originating in the second and fourth quadrants of the $\lambda$-plane pass onto the proper Riemann sheet upon crossing the generalized cutoff loci at $\omega/2\pi = 13.43 + j1.25$ GHz.

Which mode of the pair passes onto the proper sheet depends upon the path in the frequency plane. In fact, this observation is crucial to the leaky-wave analysis presented later. As also discussed later, in performing the transient analysis, we require that the Fourier (temporal) inversion contour lie in the shaded strip shown in Fig. 3. Starting at $\omega = 0$ and passing below the $\omega_n^{(1)}$ branch points (along the path $b - b'$ in Fig. 3) results in the modes originating in the first and third quadrants (for $\omega = 0$) of the $\lambda$-plane passing onto the proper Riemann sheet. This is shown in Fig. 4, where the mode trajectories for the $\mathrm{TM}_2^z$ modes $\pm\left(\lambda_2, \tilde{\lambda}_2\right)$ are shown in the complex $\lambda$-plane parameterized by frequency. Passing above the $\omega_n^{(1)}$ branch points (along the path $a - a'$ in Fig. 3) results in the modes originating in the fourth and second quadrants of the $\lambda$-plane passing onto the proper Riemann sheet, as shown in Fig. 5. For reasons discussed later the path $a - a'$ is the correct path for the leaky-wave analysis.

Near the terminus of the solid lines in Fig. 2 lie branch points that separate the $n$th mode from the negative of the $(n+2)$th mode (i.e., separates $\lambda_n(\omega)$ and $-\lambda_{n+2}(\omega)$), designated as $\omega_{n/n+2}^{(2)}$. These points connect the $n$th and $(n+2)$th modes such that a complete rotation about $\omega_{n/n+2}^{(2)}$ results in the smooth interchange of the $\pm n$th and $\mp(n+2)$th modes. As such, $\omega_{n/n+2}^{(2)}$ are first-order branch points for the $n$th and $-(n+2)$th modes. The dashed lines beginning near the $\omega_{n/n+2}^{(2)}$ points represent generalized cutoff loci where other modes change Riemann sheets, as indicated in the figure and explained in more detail in [18].

Another type of frequency-plane branch point occurs as well. The branch points $\omega_n^{(0)}$ shown in Fig. 2 denote frequency points where modes $\lambda_n(\omega)$ and $-\lambda_n(\omega)$ coalesce [18], obviously at $\lambda = 0$. These are obtained as

$$\omega_n^{(0)} = \frac{c}{2m_2n_2d}\left((n-1)\,\pi \pm j\ln\left(\frac{\frac{n_{21}}{m_{21}}+1}{\frac{n_{21}}{m_{21}}-1}\right)\right)$$

which are first-order branch points for a mode pair consisting of a mode and its negative.

The generalized cutoff frequency loci and the branch points $\omega_n^{(0)}$ and $\omega_{n/n+2}^{(2)}$ in the upper half frequency plane separate the second and fourth quadrant modes (identified relative to their "initial" location for $\omega = 0$), whereas those points and loci in the lower half frequency plane separate the first and third quadrant modes. Note that the complex frequency plane is infinitely sheeted, with branch points generally connecting only certain sheets. For TE$^z$-odd modes $\lambda_n$, $n = 1, 3, 5, \ldots$, $\omega_n^{(0)}$ and $\omega_n^{(1)}$ branch points similarly occur. In general, the aforementioned modal behavior occurs for multiple dielectric layers, with or without ground planes. Further details and numerical values for the first several branch points are provided in [18].

It is important to note that the various $\omega$-plane singularities described earlier are associated with the modal dispersion function $\lambda_n(\omega)$ and are not necessarily singularities of the field or potential itself (the effects of various singularities may cancel in the complete field representation). For instance, the branch points $\omega_n^{(0)}$ are singularities of the $n$th mode pairs and of their associated residues, as well as the sum of residues, but these points are not singularities of the deformed branch cut integrals described below. Moreover, based on causality, the Green's function must be analytic in the lower-half frequency plane.

### *B. Leaky-Wave Analysis*

In this paper, we are interested in computing the electric (magnetic) time-domain scattered potential

$$\psi^{e(m),s}(\mathbf{r},t) = F^{-1}\left\{\psi^{e(m),s}(\mathbf{r},\omega)\right\} \tag{6}$$

where $F^{-1}$ indicates an inverse temporal Fourier transform.

A vertical electric (magnetic) dipole source $(y_0 \geq 0)$

$$\mathbf{J}_{e(m)}(\mathbf{r},\omega) = \hat{y} f(\omega)\,\delta(x-x_0)\,\delta(y-y_0)\,\delta(z-z_0) \tag{7}$$

leads to $\psi^{e(m),s} = \hat{y}\psi_{yy}^{e(m),s}$, where

$$\psi_{yy}^{e(m),s}(\mathbf{r},\omega) = \frac{f(\omega)}{4\pi}\int_{-\infty}^{\infty} R_n^{e(m)}(\lambda)\,\frac{e^{-p_1(y+y_0)}}{2p_1} \times H_0^{(2)}(\lambda\rho)\,\lambda d\lambda \tag{8}$$

with $\rho = \sqrt{(x-x_0)^2+(z-z_0)^2}$. A horizontal electric (magnetic) line-source

$$\mathbf{J}_{e(m)}(\mathbf{r},\omega) = \hat{z} f(\omega)\,\delta(x-x_0)\,\delta(y-y_0) \tag{9}$$

leads to $\psi^{e(m),s}(\rho,\omega) = \hat{z}\psi_{zz}^{e(m),s}$, where

$$\psi_{zz}^{e(m),s}(\rho,\omega) = \frac{f(\omega)}{2\pi}\int_{-\infty}^{\infty} R_t^{e(m)}(\lambda)\,\frac{e^{-p_1(y+y_0)}}{2p_1} \times e^{j\lambda(x-x_0)} d\lambda \tag{10}$$

with $\lambda = k_x$ $(k_z = 0)$. The coefficients $R(\lambda)$ account for the interaction of the source with the layered medium (for a source in free-space $R = 1$). The coefficients for a grounded dielectric slab have the form

$$\begin{aligned} R_t^e(\lambda) &= \frac{m_{21}^2 p_1 - p_2 \coth(p_2 d)}{Z^{\mathrm{TE}}(\lambda,\omega)} = R_n^m(\lambda) \\ R_n^e(\lambda) &= \frac{n_{21}^2 p_1 - p_2 \tanh(p_2 d)}{Z^{\mathrm{TM}}(\lambda,\omega)} = R_t^m(\lambda) \end{aligned} \tag{11}$$

whereas for a source over multiple dielectric layers the general forms (8) and (10) are valid, although different coefficients need to be utilized. For a source embedded inside a finite layer the $(y, y')$ dependence in (8) and (10) will also be altered.

The leaky-wave analysis will be developed for the line-source case, with the point source case (8) requiring straightforward modifications. We consider the generic integral

$$\psi^s(\rho,\omega) = \frac{f(\omega)}{2\pi}\int_{-\infty}^{\infty} R(\lambda)\,\frac{e^{-p_1(y+y_0)}}{2p_1} e^{j\lambda(x-x_0)} d\lambda \tag{12}$$

where the integration path is over $\Gamma_1$, as indicated in Fig. 6.

For $(x-x_0) > 0$, complex-plane analysis and Cauchy's theorem lead to

$$\psi^s(\rho,\omega) = \frac{f(\omega)}{2\pi}\sum_{n=1}^{M}\psi_n(\rho,\lambda_n,\omega) - \frac{f(\omega)}{2\pi}\int_{\Gamma_{\mathrm{bc}}} R\,\frac{e^{-p_1(y+y_0)}}{2p_1} e^{j\lambda(x-x_0)} d\lambda \tag{13}$$

where

$$\psi_n(\rho,\lambda_n,\omega) = 2\pi j\,\frac{N(\lambda_n,\omega)}{Z'(\lambda_n,\omega)}\,\frac{e^{-p_1(y+y_0)}}{2p_1} e^{j\lambda_n(x-x_0)}$$

represents the $n$th residue, $R = (N/Z)$ indicates one of the coefficients (11), $Z' = (\partial Z(\lambda,\omega)/\partial\lambda)$, $M$ is the number of above-cutoff surface wave modes (one shown in Fig. 6), $\lambda_n$ is the propagation constant of the $n$th surface wave mode, and $\Gamma_{\mathrm{bc}}$ indicates the path around the branch cut. The contribution from the integration over $\Gamma_\infty$ vanishes by proper choice of the branch cuts associated with $p_1$, leading to $\mathrm{Re}\{p_1\} > 0$ everywhere on the top Riemann sheet of the $\lambda$-plane.

Considering the Fourier transform pair

$$\begin{aligned} \mathbf{g}(\mathbf{r},\omega) &= F\{\mathbf{g}(\mathbf{r},t)\} = \int_{-\infty}^{\infty}\mathbf{g}(\mathbf{r},t)\,e^{-j\omega t}dt \\ \mathbf{g}(\mathbf{r},t) &= F^{-1}\{\mathbf{g}(\mathbf{r},\omega)\} = \frac{1}{2\pi}\int_{-\infty-j\delta}^{\infty-j\delta}\mathbf{g}(\mathbf{r},\omega)\,e^{j\omega t}d\omega \\ &= \frac{1}{\pi}\mathrm{Re}\int_{0-j\delta}^{\infty-j\delta}\mathbf{g}(\mathbf{r},\omega)\,e^{j\omega t}d\omega \end{aligned} \tag{14}$$

where $\delta > 0$ (the last equality follows from the assumption that the time-domain quantity $\mathbf{g}(\mathbf{r},t)$ is real-valued) leads to the time-domain scattered potential $\psi^s(\rho,t) = F^{-1}\{\psi^s(\rho,\omega)\}$.

Let the ordinary Fourier inversion path in (14), parallel to and slightly below the real $\omega$-axis, be defined as $\Gamma_\omega$

$$\Gamma_\omega \equiv \{\omega : -\infty \leq \mathrm{Re}\{\omega\} < \infty, \mathrm{Im}\{\omega\} = -\delta,\ \delta > 0\} \tag{15}$$

where $\delta$ is generally taken to be small. This path is depicted in Fig. 3 as $b-b'$. To proceed with the leaky-wave analysis, we first establish the fact that since the integrand of (12) is a continuous function of both $\omega$ and $\lambda$ for $\omega \in \Gamma_\omega$ and $\lambda \in \Gamma_1$ and is a regular analytic function of $\omega$ at each point $\lambda \in \Gamma_1$, then by a well-known theorem concerning functions defined by integrals [22, pp. 107–108], $\psi^s(\rho,\omega)$ is a regular analytic function of $\omega$ for $\omega \in \Gamma_\omega$. Now, define $\Omega$ to be the horizontal strip between the $\omega_n^{(0)}$ branch points as depicted in Fig. 3

$$\Omega \equiv \left\{ \begin{array}{c} \omega : -\infty \leq \mathrm{Re}(\omega) < \infty \\ -\left|\mathrm{Im}\left(\omega_n^{(0)}\right)\right| \leq \mathrm{Im}(\omega) < \left|\mathrm{Im}\left(\omega_n^{(0)}\right)\right| \end{array} \right\}$$

for all $n > 0$. As frequency varies in this strip the location of the $\lambda$-plane singularities move correspondingly. For instance, as $\mathrm{Im}(\omega)$ becomes positive the $\lambda$-plane poles and branch points migrate across the real-$\lambda$ axis. However, by the same theorem [22, pp. 107–108] mentioned above, the path of frequency variation (i.e., the temporal transform inversion) can move about in this horizontal strip and for any such path $\psi^s(\rho,\omega)$ will be a regular analytic function of $\omega$ as long as the spatial inversion contour $\Gamma_1$ stays on the same side of the $\lambda$-plane singularities as these points migrate with varying frequency. For example, if frequency is varied along the path $b-b'$ in Fig. 3, the spatial inversion contour is $\Gamma_1$ as shown in Fig. 6, but if frequency is varied along the path $a-a'$ in Fig. 3, the spatial inversion contour $\Gamma_1$ must be deformed to stay above the migrating singular-

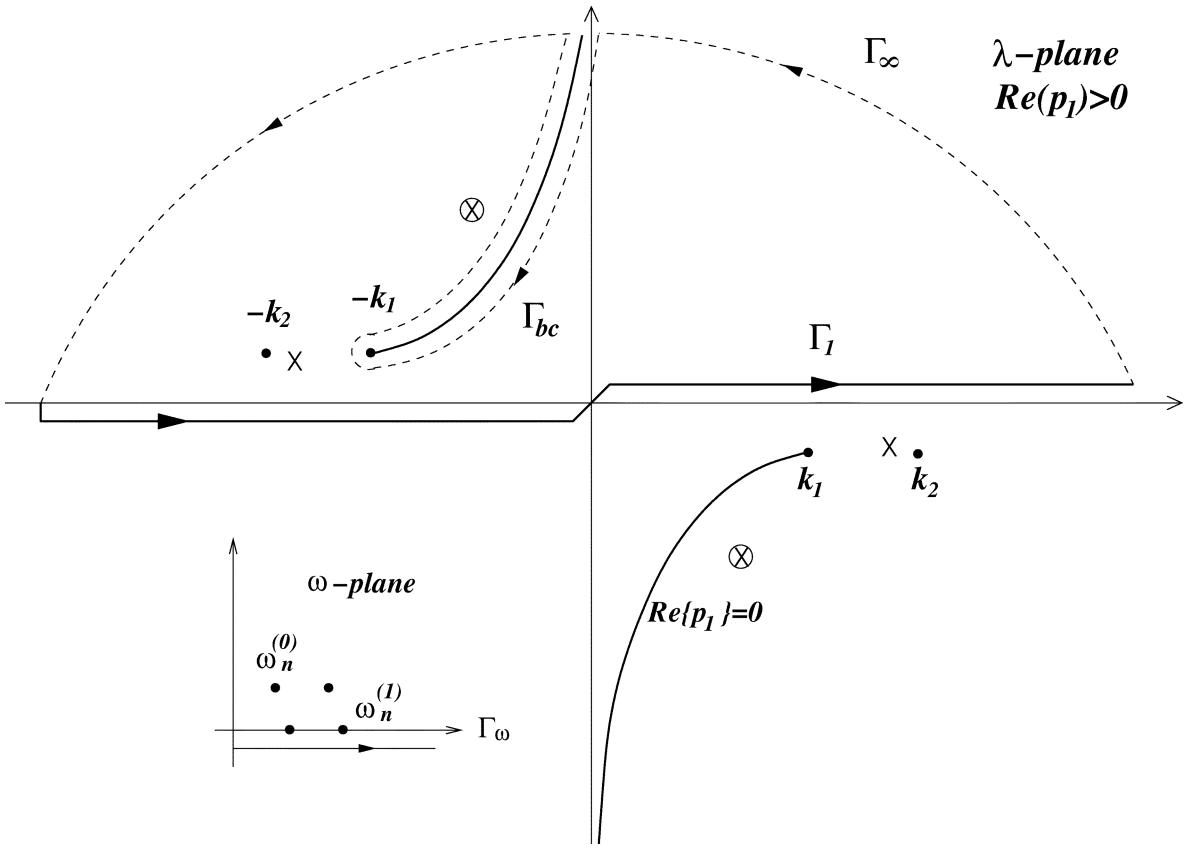


Fig. 6. Complex analysis in the $\lambda$-plane for evaluation of (12) leading to (13). Original integration contour $\Gamma_1$ is deformed into the upper-half plane for $(x-x_0)>0$ such that the integral (12) is found as a branch cut integral and a sum of residues via Cauchy's theorem. "$X$" denotes proper, above-cutoff surface-wave modes (one shown), and "$\otimes$" denotes improper, below-cutoff surface wave modes, located on the bottom sheet (one shown). The insert depicts the contour of frequency variation $\Gamma_\omega$, which is below the real-axis branch point singularities $\omega_n^{(1)}$, where all branch point singularities are depicted as solid dots in the insert.

ities, as shown in Fig. 7. Therefore, we may deform the path $\Gamma_\omega$ into the path $a-a'$ in Fig. 3, defined to be $\Gamma_\omega^u$

$$\Gamma_\omega^u \equiv \left\{ \begin{array}{c} \omega : -\infty \le \mathrm{Re}\,\{\omega\} < \infty, \mathrm{Im}\,\{\omega\} = \delta > 0 \\ \mathrm{Im}\left(\omega_n^{(1)}\right) < \delta < \left|\mathrm{Im}\left(\omega_n^{(0)}\right)\right| \end{array} \right\}. \quad (16)$$

For reasons described later, we take $\Gamma_\omega^u$ as the Fourier inversion contour in the leaky-wave analysis to follow.

Now, as frequency is varied along the temporal inversion contour $\Gamma_\omega^u$, the branch-cut integral may be discontinuous as surface-wave modes cross the branch cut and move from the improper to the proper Riemann sheet in the $\lambda$-plane. When this happens, the surface-wave mode begins to contribute to $\psi^s(\rho,\omega)$ as a residue contribution in the discrete summation, offsetting the discontinuity in the branch cut integral and maintaining continuity of $\psi^s(\rho,\omega)$.

It order to make the integral (branch cut) contribution to $\psi^s(\rho,t)$ vanish, which is the goal of the leaky-wave formulation, it is necessary to make $\psi^s(\rho,\omega)$ an entire function in the upper-half $\omega$-plane. Following [12], additional integration segments $-\int_{\Gamma_{\mathrm{IP}}}(\cdot)\,d\lambda$ on the improper $\lambda$-plane sheet are added to the branch-cut integration in (13). The contour $\Gamma_{\mathrm{IP}}$ encloses in a counter-clockwise direction the improper modes which eventually become proper modes and is such that the new contour $\Gamma_{\mathrm{bc}}+\Gamma_{\mathrm{IP}}$ is never crossed as modes migrate from the improper sheet onto the proper Riemann sheet. The deformed contour $\Gamma_1$ as well as the deformed branch cut is depicted in Fig. 7. The resulting integral $-\int_{\Gamma_{\mathrm{bc}}+\Gamma_{\mathrm{IP}}}(\cdot)\,d\lambda$ will then be continuous as a function of frequency and is, in fact, an entire function of $\omega$ in the upper-half frequency plane as described in [12, App.]. The additional contribution to (13) from the integration $-\int_{\Gamma_{\mathrm{IP}}}(\cdot)\,d\lambda$ is offset by including residues $\sum_{n=M+1}^{\infty}$ in the summation corresponding to the improper modes encircled by the paths $\Gamma_{\mathrm{IP}}$, leading to

$$\psi^s(\rho,\omega) = \frac{f(\omega)}{2\pi}\sum_{n=1}^{\infty}\psi_n(\rho,\lambda_n,\omega) - \frac{f(\omega)}{2\pi}\int_{\Gamma_{\mathrm{bc}}+\Gamma_{\mathrm{IP}}} R\frac{e^{-p_1(y+y_0)}}{2p_1}e^{j\lambda(x-x_0)}d\lambda \quad (17)$$

for $\omega\in\Gamma_\omega^u$, where the summation includes all proper modes and all improper modes originating in the second quadrant of the $\lambda$-plane for sufficiently low frequency $\mathrm{Re}\,(\omega)\ll\omega_n^c$ (these are analytically continuous to proper modes; see Fig. 5). The integration is now over $\Gamma_{\mathrm{bc}}+\Gamma_{\mathrm{IP}}$, which includes the branch-cut on the top Riemann sheet and the excursions around the improper surface-wave modes on the bottom sheet as shown in Fig. 7 (one shown). The summation and integration in (17) are now separately continuous functions of $\omega$.

The new inversion contour $\Gamma_\omega^u$ is used rather than the usual Fourier inversion contour $\Gamma_\omega$ because, as described in Section II-A, as frequency varies along $\Gamma_\omega$, it is the improper modes originating in the first and third quadrants of the $\lambda$-plane which eventually emerge as proper surface-wave modes (for large

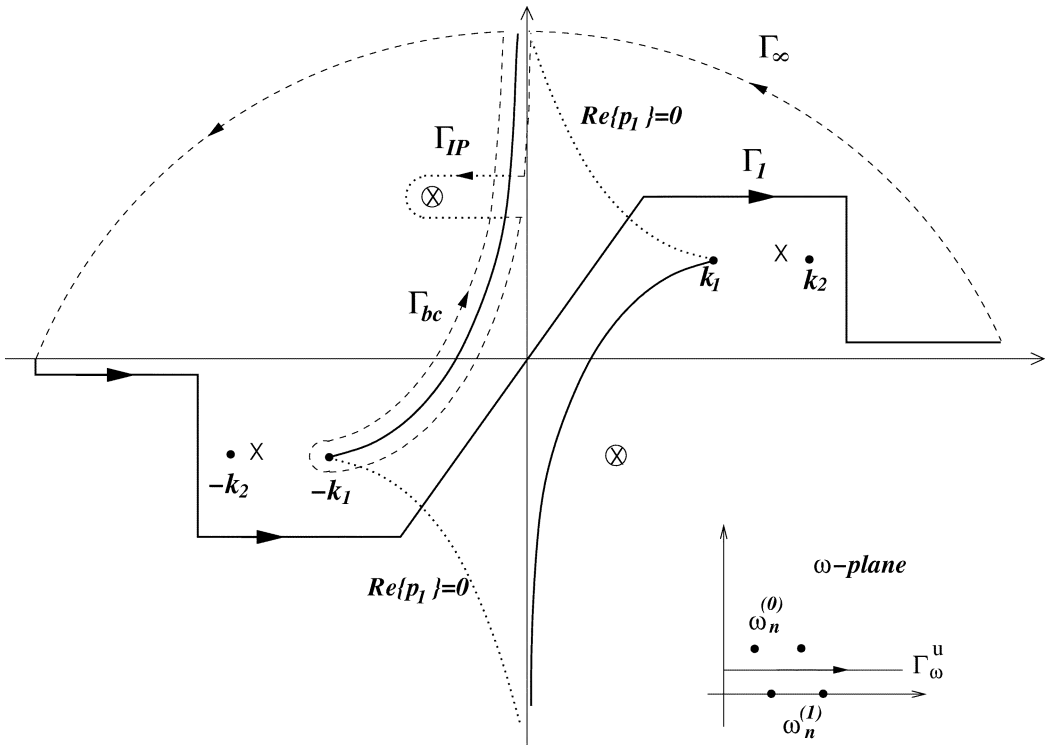


Fig. 7. Complex analysis in $\lambda$-plane for evaluation of (12) leading to (17). Original integration contour $\lambda_1$ is deformed into the upper-half plane for $(x-x_0)>0$ such that the integral (12) is found as a branch cut integral over $\Gamma_{\rm bc}$ on the top sheet, and integral over contour $\Gamma_{\rm IP}$ on the bottom sheet, and an infinite sum of residues, both proper "$X$" on the top sheet and improper "$\otimes$" on the bottom sheet. The insert depicts the contour of frequency variation $\Gamma_\omega^u$, which is below the upper $\omega_n^{(0)}$ branch points but above the real-axis branch points $\omega_n^{(1)}$.

$\mathrm{Re}\,(\omega)$ ultimately residing in the forth and second quadrants of the $\lambda$-plane, respectively, see Fig. 4). Noting that modes $\lambda_n$ in the third quadrant are such that $\mathrm{Im}\,(\lambda_n)\to-\infty$ as $n\to\infty$ for the TM$^z$-even modes, and for all $n$ for the TE$^z$-odd modes, the factor $e^{j\lambda_n(x-x_0)}=e^{j\mathrm{Re}(\lambda_n)(x-x_0)}e^{-\mathrm{Im}(\lambda_n)(x-x_0)}$ is unbounded and the summation over improper modes will not converge [for $(x-x_0)<0$ the same problem arises with the first quadrant modes, which are captured by the necessary lower-half $\lambda$-plane closure]. However, as frequency varies along $\Gamma_\omega^u$ it is the improper modes which originate in the second and forth quadrants of the $\lambda$-plane which eventually become the above-cutoff proper modes [in this case for large $\mathrm{Re}\,(\omega)$ ultimately residing in the third and first quadrants of the $\lambda$-plane, respectively; see Fig. 5], leading to a convergent sum in (17). All TE$^z$-odd and TM$^z$-even modes have similar behavior excepting the first TM mode which does not have a low-frequency cutoff. Note that the temporal integration contour is located within the strip shown in Fig. 3 since in passing outside of this strip the $\omega_n^{(0)}$ branch points are encircled, leading to an interchange of each mode with its negative, which leads to the wrong mode being captured in the residue evaluation.

It is important to note that the correct $\lambda$-plane branch cuts to choose for $\omega\in\Gamma_\omega^u$ are shown in Fig. 7 (solid lines emanating from $\pm k_1$) and are the cuts that are smoothly continuous to the usual hyperbolic cuts for $\omega\in\Gamma_\omega$ shown in Fig. 6. These correct cuts are not the "proper" cuts that are defined by $\mathrm{Re}\,(p_1)=0$ and that would result in the top sheet being everywhere proper (for illustrative purposes these "proper" cuts are also shown in Fig. 7 as dotted lines emanating from $\pm k_1$). The central area in Fig. 7 formed by the boundaries of the "proper" cuts and the correct cuts for this problem has $\mathrm{Re}\,(p_1)<0$ on the top sheet, whereas outside of this area on the top sheet $\mathrm{Re}\,(p_1)>0$. Even though the radiation condition is not satisfied everywhere on the top Riemann sheet (which is at some level commiserate with the fact that we invoke leaky modes), the correctness of the branch cuts shown in Fig. 7 can be deduced from the requirement that continuity must be maintained as the frequency-plane path is deformed. As the $\lambda$-plane branch points at $\lambda=\pm k_1$ migrate across the real-$\lambda$ axis, the spatial inversion path $\Gamma_1$ is moved correspondingly to remain on the same side of the $\lambda$-plane branch points, to maintain continuity. For this reason, the branch cut in the right-half $\lambda$-plane, for instance, must continue to be below the path $\Gamma_1$, as shown in Fig. 7. Also note that the "proper" cuts suddenly flip direction as the branch point crosses the real-$\lambda$ axis, and if allowed to do so would suddenly cross the $\Gamma_1$ inversion contour, leading to a discontinuity. Furthermore, the correct branch cut must also approach the line $\mathrm{Re}\,(\lambda)=0$ as $\mathrm{Im}\,(\lambda)\to\pm\infty$ in order for the contribution from $\Gamma_\infty$ to vanish via Jordan's lemma, and so vertical branch-cuts, which were described in [12] and [16], are not appropriate.

In order to eliminate the integral contribution in (17) and determine the resulting time-domain scattered potential as a discrete sum of modes, two characteristic times are defined. Define $\tau_e$ as the least-travel time for a disturbance from the source to reach the observer subsequent to specular reflection from the air-dielectric interface, and $\tau_l$ as the least-travel time for a disturbance from the source to reach the observer subsequent to the first reflection from the ground plane. It is easy to see that $\tau_e=m_1n_1\sqrt{(x-x_0)^2+(y+y_0)^2+(z-z_0)^2}/c$.

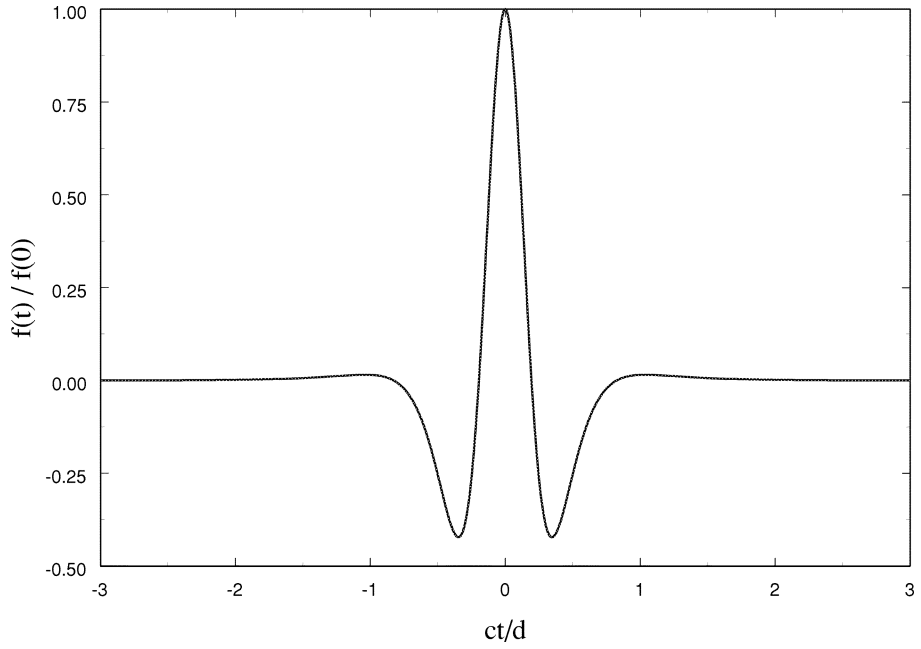


Fig. 8. Temporal behavior of Rayleigh wavelet source $t_i = 0.6d/c$.

Note that any of the coefficients in (11) can be written as

$$\begin{aligned} R =& \pm \frac{K + e^{-2p_2 d}}{1 + Ke^{-2p_2 d}} \\ =& \pm \frac{K}{1 + Ke^{-2p_2 d}} \pm \frac{e^{-2p_2 d}}{1 + Ke^{-2p_2 d}} \\ =& R_{et} + R_{lt} \end{aligned} \tag{18}$$

where $K$ is introduced in the Appendix [see (24)] and the first term $R_{et}$ represents an early-time reflection coefficient (involving the specular reflection from the air-dielectric interface of the grounded dielectric slab via the numerator $K$). The potential (17) is written as

$$\begin{aligned} \psi^s(\rho,\omega) =& \frac{f(\omega)}{2\pi} \sum_{n=1}^{\infty} \psi_n(\rho, \lambda_n, \omega) \\ & - \frac{f(\omega)}{2\pi} \int_{\Gamma_{\rm bc}+\Gamma_{\rm IP}} R_{et} \frac{e^{-p_1(y+y_0)}}{2p_1} \\ & \times e^{j\lambda(x-x_0)} d\lambda \\ & - \frac{f(\omega)}{2\pi} \int_{\Gamma_{\rm bc}+\Gamma_{\rm IP}} R_{lt} \frac{e^{-p_1(y+y_0)}}{2p_1} \\ & \times e^{j\lambda(x-x_0)} d\lambda. \end{aligned} \tag{19}$$

The integral associated with $R_{et}$ will be called the early-time branch cut, whereas the integral associated with $R_{lt}$ will be called the late-time branch cut.

For $t < \tau_e$ it is obvious that $F^{-1}\{\psi^s(\rho,\omega)\} = 0$. As described in the Appendix, for $\tau_e \le t < \tau_l$, the contribution from the early-time branch cut integral in (19) vanishes, and the contribution from the late-time branch cut integral in (19) cancels with the corresponding residue term (the residue term associated with $R_{lt}$). The complete early-time transient potential is computed as

$$\begin{aligned} \psi^s_{et}(\rho,t) =& \frac{1}{\pi} \sum_{n=1}^{\infty} {\rm Re} \int_{0-j\delta}^{\infty-j\delta} e^{j\omega t} \frac{f(\omega)}{2\pi} \\ & \times \psi_n(\rho, \lambda_n, \omega)\big|_{R=R_{et}} d\omega \\ =& \frac{f(t)}{2\pi} * \sum_{n=1}^{\infty} \psi_{et,n}(\rho,t) \end{aligned} \tag{20}$$

where $\psi_{et,n}(\rho,t) = F^{-1}\{\psi_n(\rho,\lambda_n,\omega)|_{R=R_{et}}\}$, which represents the transient residue contribution from the $n$th surface wave mode. In (20), only the first term $(R_{et})$ of (18) is used, and we denote this as the early-time residue series. For this term ${\rm Re}\{p_2\} < 0$, although the sign of $p_2$ is immaterial for the coefficient $R = R_{et} + R_{lt}$.

For $t \ge \tau_l$, it is shown in Appendix that the contributions from both integrals in (19) vanish, and the complete transient potential is computed from

$$\begin{aligned} \psi^s_{lt}(\rho,t) =& \frac{1}{\pi} \sum_{n=1}^{\infty} {\rm Re} \int_{0-j\delta}^{\infty-j\delta} e^{j\omega t} \cdot \frac{f(\omega)}{2\pi} \\ & \times \psi_n(\rho, \lambda_n, \omega)\big|_{R=R_{et}+R_{lt}} d\omega \\ =& \frac{f(t)}{2\pi} * \sum_{n=1}^{\infty} \psi_n\big|_{R=R_{et}+R_{lt}}(\rho,t) \end{aligned} \tag{21}$$

using the coefficient $R = R_{et} + R_{lt}$, which is henceforth called the late-time residue series, leading to the late-time potential $\psi^s_{lt}$. The final waveform as calculated via the leaky-wave analysis is then given as

$$\psi^s(t) = \psi^s_{et}[H(t-\tau_e) - H(t-\tau_l)] + \psi^s_{lt} H(t-\tau_l) \tag{22}$$

where $H$ is the usual Heaviside function.

In general, $\psi_n(\rho,t)$ will include both proper and improper spectral contributions. For $(x - x_0) < 0$ and for the

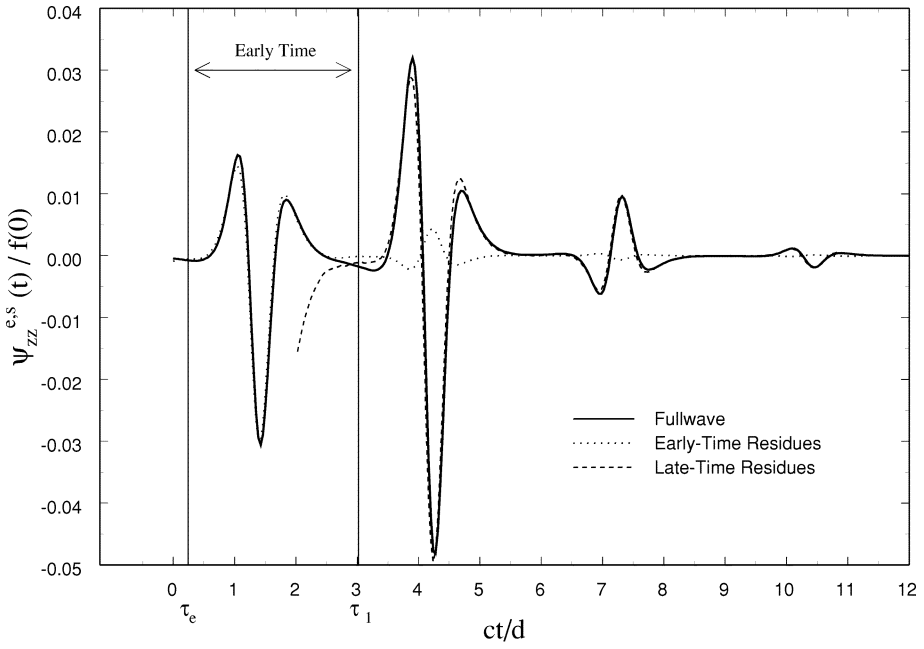


(a)

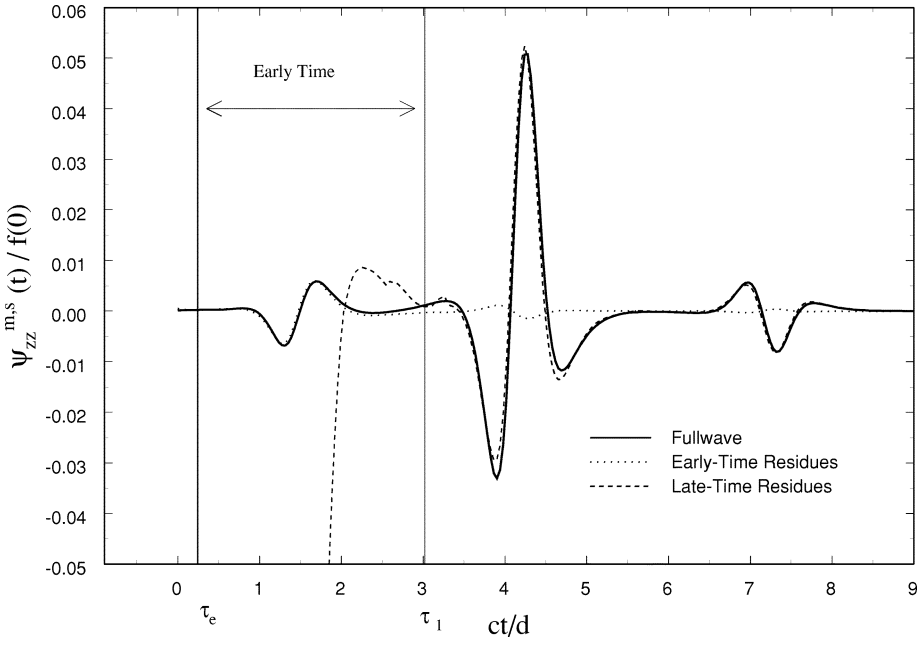


(b)

Fig. 9. Scattered transient potentials computed via fullwave and leaky-mode methods for a grounded slab having $n_1 = m_1 = 1$ (air), $n_2 = 1.6$, $m_2 = 1$, $d = 3.33$ cm, $(x_0, y_0, z_0) = (0, 2, 0)$ cm, $(x, y, z) = (4, 0, 0)$ cm. (a) $\psi_{zz}^{e,s}$ due to an electric line-source. (b) $\psi_{zz}^{m,s}$ due to a magnetic line-source.

point-source solution (8), the $\lambda$-plane path $\Gamma_1$ is closed in the lower-half plane. For the point-source case an analogous method leads to $\psi^s(\mathbf{r}, t) = (f(t)/4\pi) * \sum_{n=1}^{\infty} \psi_n(\mathbf{r}, t)$. Note that in (20) we have interchanged the order of the inversion integral and the summation, which is acceptable assuming that the series is appropriately convergent.

## III. Results and Discussion

The geometry is depicted in Fig. 1, showing a source located at $(x_0, y_0, z_0)$ and observation point $(x, y, z)$. The time-dependence of the source is chosen as the Rayleigh wavelet [3]

$$f(t) = \frac{t_i^4}{24\pi}\mathrm{Re}\left\{\frac{\partial^4}{\partial t^4}\frac{1}{jt}\right\} = \frac{t_i^4}{\pi}\mathrm{Im}\left\{\frac{1}{t^5}\right\}$$

where $t = t_r - jt_i$, such that $f(\omega) = (t_i^4\omega^4/24)e^{-|\omega|t_i}$. For the results shown here $t_i = 0.6d/c$, with the normalized source waveform shown in Fig. 8.

In all figures, the scattered transient potentials are shown. In Fig. 9, transient potentials computed via fullwave (double numerical integration) and leaky-mode methods are shown for a grounded slab having $n_1 = m_1 = 1$ (air), $n_2 = 1.6$, $m_2 = 1$,

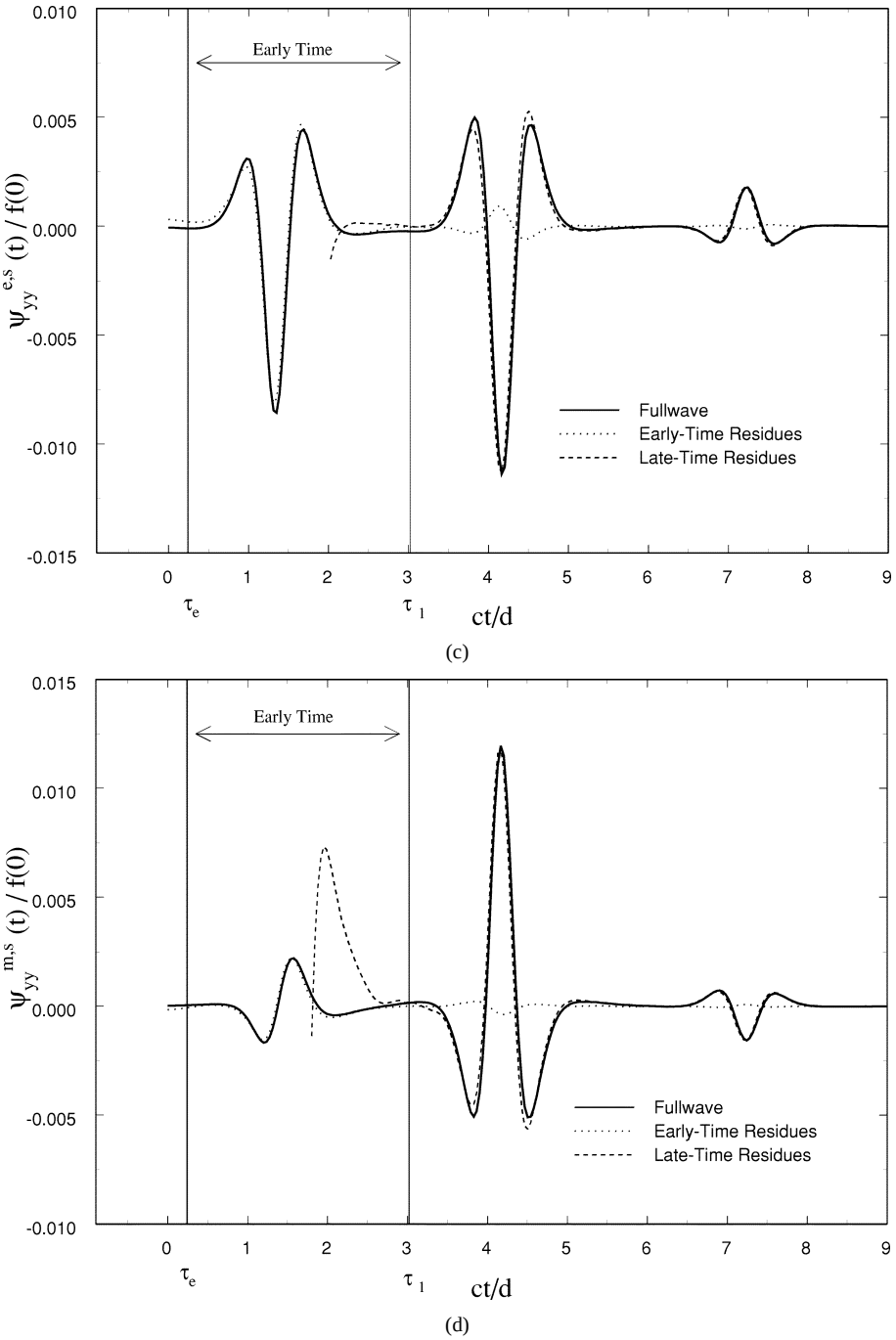


Fig. 9. (*Continued.*) Scattered transient potentials computed via fullwave and leaky-mode methods for a grounded slab having $n_1 = m_1 = 1$ (air), $n_2 = 1.6$, $m_2 = 1$, $d = 3.33$ cm, $(x_0, y_0, z_0) = (0, 2, 0)$ cm, $(x, y, z) = (4, 0, 0)$ cm. (c) $\psi_{yy}^{e,s}$ due to an electric dipole. (d) $\psi_{yy}^{m,s}$ due to a magnetic dipole.

$d = 3.33$ cm, $(x_0, y_0, z_0) = (0, 2, 0)$ cm, and $(x, y, z) = (4, 0, 0)$ cm. In Fig. 9(a), the normalized potential $\psi_{zz}^{e,s}/f(0)$ is shown for an electric line-source. Note that during early-time the early-time residue series is in very good agreement with the fullwave method. Alternately, the early-time potential could also be computed using the fullwave method with the coefficient $R$ corresponding to that of a single interface, since this wavefront corresponds to the specular reflection from the top interface of the slab. In fact, this single interface (early-time) response can be determined in closed form [21].

Late time begins when the reflection from the ground plane reaches the observer. The time-interval from source to receiver via this path is calculated as $ct/d = 4.168$, yet the source actually turns on at approximately $ct/d = -1.1$, and so the arrival from the ground-plane reflection should occur at approximately $ct/d = 3.068$, as indicated in the figure. Note that the turn-on time for this particular source is somewhat difficult to specify. The waveform in Fig. 8 exhibits a slight peak around $ct/d = -1.1$ (not shown due to the scale of the figure) before falling steeply to negative values, and this peak was chosen as the turn-on time for the waveform.

During late-time, the late-time residue series agree very well with the fullwave (double numerical integration) method. It should be emphasized that for $\tau_e < t < \tau_l$, the late-time

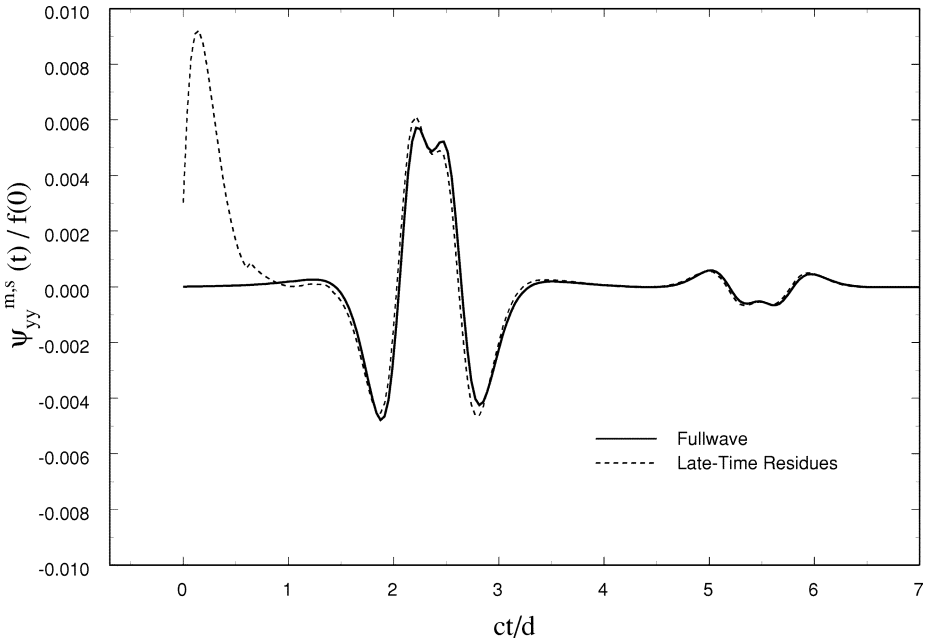


Fig. 10. Scattered transient potential $\psi_{yy}^{m,s}$ inside the grounded slab due to a magnetic dipole outside the slab computed via fullwave and leaky-mode methods, $n_1 = m_1 = 1$ (air), $n_2 = 1.6$, $m_2 = 1$, $d = 3.33$ cm, $(x_0, y_0, z_0) = (0, 2, 0)$ cm, $(x, y, z) = (2, -3, 0)$ cm. In this case, the observation point is sufficiently near the ground plane to allow modes to establish themselves by the time the first wavefield reaches the observation point.

residues cancel with the associated late-time branch cut contribution. These residues are nevertheless plotted in this time interval so that it may be observed that at $\tau = \tau_l$, they begin to represent the correct solution (for $t > \tau_l$ the late-time branch cut vanishes).

In Fig. 9(a)–(d), similar results are shown for a magnetic line-source, an electric point-source, and a magnetic point-source, respectively. In all cases the leaky-wave solution agrees with the fullwave solution during the appropriate time interval.

It should be noted that this type of behavior, where the late-time or full residue series begins to agree with the fullwave solution at the onset of late-time is identical to that observed in the singularity-expansion method (SEM) literature [23] (see, e.g., the figures in [24]), which was originally developed to evaluate plane-wave transient scattering from objects. While the leaky-wave analysis presented here is not SEM, it has some resemblance to SEM since both methods utilize complex frequency-plane singularities and Cauchy's theorem to evaluate transient fields. In [25], the SEM analysis of plane-wave scattering from a grounded slab is presented. Similar early-time and late-time concepts are found to be necessary, including the decomposition of fields into two terms, each of which is evaluated by closure of the frequency-domain inversion contour by semicircles in opposing half-planes as described in the Appendix. Since the work in [25] concerns a plane-wave scattering problem, and here we consider a near-field diffraction problem, it is not surprising that the governing physics is somewhat similar.

In Fig. 10, the transient potential $\psi_{yy}^{m,s}$ evaluated inside a grounded slab at $(x, y, z) = (2, -3, 0)$ cm due to a magnetic dipole source outside the slab at $(x_0, y_0, z_0) = (0, 2, 0)$ cm is shown. In this case, the observation point is sufficiently near to the ground plane to allow modes to establish themselves by the time the first wavefield reaches the observation point, and there is no need for the concept of early-time.

It can be seen that the leaky-wave method leads to an efficient computation of the transient potential, which necessitates only the numerical evaluation of rapidly convergent one-dimensional (1-D) integrals. The number of modes required for an accurate solution is often quite small and will depend both on the geometry and the driving source function in question. For example, although 30 modes were used to generate the numerical results shown in Fig. 9, ten modes yielded essentially the same result. Even fewer modes lead to good accuracy for the early-time response. In the numerical solution, the dispersion behavior of these modes was precomputed once for the geometry of interest, which took just a few seconds on a modern personal computer. For the fullwave results the potential was calculated over the contour $\Gamma_\omega(15)$ with $\delta/c = 0.05$, and for the leaky-wave results the potential was calculated over the contour $\Gamma_\omega^u(16)$ with $\delta/c = 0.05$ $\left(0 < \mathrm{Im}\,(\omega) < \mathrm{Im}\left(\omega_n^{(0)}/c\right) = 0.1376\right)$.

It is difficult to directly compare computation times, since no effort was made to optimize the fullwave computation. However, the leaky-mode method, which entails a 1-D integration of a rapidly convergent series, was more than an order of magnitude faster than the fullwave computation. Note also that the final expression (22) is very easy to compute, involving simply a sum over all proper surface waves and all improper modes originating in quadrant two (four) in the wavenumber plane for the line-source (point-source) cases.

## IV. Conclusion

In this paper, we have presented a method to compute the transient potential due to currents in layered media using a leaky-wave analysis. The method relies on properties of the proper and improper surface-wave modes when frequency is analytically continued into the complex frequency plane. It was shown that this method is efficient and physically insightful,

consisting simply of an inverse temporal transform of a modal residue series. The concept of early-time and late-time intervals was presented, similar to that found in the SEM literature. It was shown that the leaky-wave method can be correctly formulated for all time intervals of interest if the reflection coefficient occurring in the residue series is appropriately modified for early-time. Numerical results were presented which demonstrate the accuracy of the method.

## APPENDIX

### VANISHING OF THE BRANCH CUT COMPONENT

Here we show that for $t \geq \tau_e$ the transient response due to a canonical source can be expressed purely as a inverse Fourier transform of a residue series. We consider an electric line-source; details for the other three cases of interest follow in a similar fashion.

We rewrite the reflection coefficient $R_t^e$ as

$$R_t^e = \frac{m_{21}^2 p_1 - p_2 \coth(p_2 d)}{m_{21}^2 p_1 + p_2 \coth(p_2 d)} \tag{23}$$

$$= -\frac{K + e^{-2p_2 d}}{1 + K e^{-2p_2 d}} \tag{24}$$

where $K = (p_2 - m_{21}^2 p_1/p_2 + m_{21}^2 p_1)$. Upon introducing the ray parameter $p = \lambda/\omega$ in the spatial-wavenumber branch cut integrals in (19), these integrals take the form

$$\frac{1}{2\pi} \int_{\Gamma_\omega^u} e^{j\omega t} \omega \frac{f(\omega)}{2\pi} L(\omega)\, d\omega \tag{25}$$

where

$$L(\omega) = L_e(\omega) + L_l(\omega) = \int_{\Gamma_p} \Phi_e(\omega, p)\, e^{-j\omega\chi_e(p)} dp + \int_{\Gamma_p} \Phi_l(\omega, p)\, e^{-j\omega\chi_l(p)} dp \tag{26}$$

with $\Gamma_p$ as the mapping of the branch-cut contour $\Gamma_{\rm bc} + \Gamma_{\rm IP}$ into the $p$-plane, $\zeta_i = \sqrt{(m_i^2 n_i^2/c^2) - p^2}$, $i = 1, 2$, $K = (\zeta_2 - m_{21}^2 \zeta_1/\zeta_2 + m_{21}^2 \zeta_1)$, $\chi_e = -p(x - x_0) + \zeta_1(y + y_0)$, $\chi_l = -p(x - x_0) + \zeta_1(y + y_0) + 2\zeta_2 d$, $\Phi_e(\omega, p) = (K/1 + K e^{-j2\omega\zeta_2 d})(1/2j\omega\zeta_1)$, and $\Phi_l(\omega, p) = (1/1 + K e^{-j2\omega\zeta_2 d})(1/2j\omega\zeta_1)$.

We consider closing the integral contour in (25) with a semicircle either in the upper-half or lower-half complex frequency plane. In order to justify this closure and to pick the appropriate half-plane (upper or lower), we approximate (26) for $|\omega| \to \infty$ using the method of steepest descents. Assuming that $\Phi_{e,l}$ is slowly varying compared to the exponential term $e^{-j\omega\chi_{e,l}}$, we approximate (26) as

$$L(\omega) = \Phi_e(\omega, p_e^s) \sqrt{\frac{2\pi}{j\omega\chi_e''(p_e^s)}} e^{-j\omega\chi_e(p_e^s)} + \Phi_l(\omega, p_l^s) \sqrt{\frac{2\pi}{j\omega\chi_l''(p_l^s)}} e^{-j\omega\chi_l(p_l^s)} \tag{27}$$

where the saddle-point $p_{e,l}^s$ satisfies the condition $\chi_{e,l}'\left(p_{e,l}^s\right) = 0$. The early-time saddle-point is

$$p_e^s = -\frac{m_1 n_1}{c} \frac{(x - x_0)}{\sqrt{(x - x_0)^2 + (y - y_0)^2}}$$

and the position for the late-time saddle-point can be shown to obey $-m_1 n_1/c < p_l^s \leq 0$. Note that $\tau_e = \chi_e(p_e^s, x, y)$ and $\tau_l = \chi_l(p_l^s, x, y)$. It is easy to check the special case $x = x_0$ such that $p_{e,l}^s = 0$, and therefore, $\chi_e(0, x_0, y) = m_1 n_1/c(y + y_0)$ and $\chi_l(0, x_0, y) = (m_1 n_1/c)(y + y_0) + (m_2 n_2/c)2d$, which clearly define times associated with the reflection from the dielectric interface and the ground plane, respectively.

The integrand of (25) then becomes

$$\sqrt{\frac{2\pi}{j\chi_e''(p_e^s)}} \sqrt{\omega} \frac{f(\omega)}{2\pi} \Phi_e(\omega, p_e^s)\, e^{j\omega(t - \chi_e(p_e^s))} + \sqrt{\frac{2\pi}{j\chi_l''(p_l^s)}} \sqrt{\omega} \frac{f(\omega)}{2\pi} \Phi_l(\omega, p_l^s)\, e^{j\omega(t - \chi_l(p_l^s))}. \tag{28}$$

For $\tau_e < \tau < \tau_l$, we consider the two terms in (28) separately. For the first term, which is associated with early-time, based on the factor $e^{j\omega(t - \chi_e(p_e^s))} = e^{j\omega(t - \tau_e)}$, we close the Fourier inversion path $\Gamma_\omega^u$ with a semicircle of infinite radius in the upper-half frequency plane. There is no contribution from the integral over the infinite semicircle. Since the branch cut integral is a regular analytic function in the upper-half frequency plane as described previously, the transient contribution from the first term in (28) vanishes.

For the second term in (28), which is associated with late-time, the factor $e^{j\omega(t - \chi_l(p_l^s))} = e^{j\omega(t - \tau_l)}$ dictates closure of the Fourier inversion path $\Gamma_\omega^u$ in the lower-half frequency plane, with no contribution from the integration over the infinite semicircle. However, the branch cut integral $L(\omega)$ is not necessarily analytic in the lower-half frequency plane, and so by Cauchy's theorem, there is a nonzero contribution to the transient response. However, this nonzero contribution must cancel with the associated term in the leaky-mode residue summation (associated with the partial reflection coefficient $R_{lt}$) since it can be shown, using (12) with $R = R_{lt}$, that the scattered potential associated with $R_{lt}$ identically vanishes for $t < \tau_l$. Therefore, during this time period the complete transient response is given by (20).

For $t > \tau_l$, we close the Fourier inversion path $\Gamma_\omega^u$ in the upper-half frequency plane for both terms, based on the exponential factors in (28), such that during this time period the entire branch cut integral vanishes, and the complete transient response is given by (21). Note that in this analysis we have assumed $f(\omega) = O(1)$ for simplicity.

## ACKNOWLEDGMENT

The authors would like to acknowledge helpful discussions with R. A. W. Haddon and D. G. Duffy concerning their related work.

## REFERENCES


[1] L. Tsang and J. A. Kong, "Modified modal theory of transient response in layered media," *J. Math Phys*, vol. 20, no. 6, pp. 1170–1182, June 1979.

[2] A. Ezzeddine, J. A. Kong, and L. Tsang, "Time response of a vertical electric dipole over a two-layer medium by the double deformation technique," *J. Appl. Phys*, vol. 53, no. 2, pp. 813–822, Feb. 1982.

[3] L. B. Felsen and F. Niu, "Spectral analysis and synthesis options for short pulse radiation from a point dipole in a grounded dielectric layer," *IEEE Trans. Antennas Propagat.*, vol. 41, pp. 747–754, June 1993.

[4] F. Niu and L. B. Felsen, "Time-domain leaky modes on layered media: Dispersion characteristics and synthesis of pulsed radiation," *IEEE Trans. Antennas Propagat.*, vol. 41, pp. 755–761, June 1993.

[5] ——, "Asymptotic analysis and numerical evaluation of short pulse radiation from a point dipole in a grounded dielectric layer," *IEEE Trans. Antennas Propagat.*, vol. 41, pp. 762–769, June 1993.

[6] A. T. deHoop, "Pulsed electromagnetic radiation from a line source in a two-media configuration," *Radio Sci.*, vol. 14, no. 2, pp. 253–268, Mar.–Apr. 1979.

[7] E. F. Kuester, "The transient electromagnetic field of a pulsed line source located above a dispersively reflecting surface," *IEEE Trans. Antennas Propagat.*, vol. AP-32, pp. 1154–1162, Nov. 1984.

[8] R. Dai and C. T. Young, "Transient fields of a horizontal electric dipole on a multilayered dielectric medium," *IEEE Trans. Antennas Propagat.*, vol. 45, pp. 1023–1031, June 1997.

[9] D. A. Hill, "The transient fields of a Hertzian dipole in the presence of a dielectric half-space," *Radio Sci.*, vol. 6, no. 8,9, pp. 787–794, Aug.–Sept. 1971.

[10] K. I. Nikoskinen and I. V. Lindell, "Time-domain analysis of the Sommerfeld VMD problem based on the exact image theory," *IEEE Trans. Antennas Propagat.*, vol. 38, pp. 241–250, Feb. 1990.

[11] K. I. Nikoskinen, "Time-domain analysis of horizontal dipoles in front of planar dielectric interface," *IEEE Trans. Antennas Propagat.*, vol. 38, pp. 1951–1957, Dec. 1990.

[12] R. A. W. Haddon, "Exact evaluation of the response of a layered elastic medium to an explosive point source using leaking modes," *Bull. Seism. Soc. Amer.*, vol. 76, no. 6, pp. 1755–1775, Dec. 1986.

[13] ——, "Response of an oceanic wave guide to an explosive point source using leaking modes," *Bull. Seism. Soc. Amer.*, vol. 77, no. 5, pp. 1804–1822, Oct. 1987.

[14] ——, "Numerical evaluation of Green's functions for axisymmetric boreholes using leaking modes," *Geophys.*, vol. 52, no. 8, pp. 1099–1105, Aug. 1987.

[15] ——, "Exact Green's functions using leaking modes for axisymmetric boreholes in solid elastic media," *Geophys.*, vol. 54, no. 5, pp. 609–620, May 1989.

[16] D. G. Duffy, "Response of a grounded dielectric slab to an impulsive line source using leaky modes," *IEEE Trans. Antennas Propagat.*, vol. 42, pp. 340–346, Mar. 1994.

[17] R. E. Collin, *Field Theory of Guided Waves*, 2nd ed. New York: IEEE, 1991, ch. 11.

[18] G. W. Hanson and A. B. Yakovlev, "Investigation of mode interaction on planar dielectric waveguides with loss and gain," *Radio Sci.*, vol. 34, no. 6, pp. 1349–1359, Nov.–Dec. 1999.

[19] ——, "An analysis of leaky-wave dispersion phenomena in the vicinity of cutoff using complex frequency plane singularities," *Radio Sci.*, vol. 33, no. 4, pp. 803–820, July–Aug. 1998.

[20] J. S. Bagby and D. P. Nyquist, "Dyadic Green's functions for integrated electronic and optical circuits," *IEEE Trans. Microwave Theory Tech.*, vol. MTT-35, pp. 206–210, Feb. 1987.

[21] W. C. Chew, *Waves and Fields in Inhomogeneous Media*. New York: IEEE, 1990.

[22] E. T. Copson, *Theory of Functions of a Complex Variable*. London, U.K.: Oxford Univ Press, 1935, p. 107.

[23] C. E. Baum, "The singularity expansion method," in *Transient Electromagnetic Fields*, L. B. Felson, Ed. New York: Springer-Verlag, 1976, pp. 128–177.

[24] J. E. Ross, E. J. Rothwell, D. P. Nyquist, and K. M. Chen, "Transient coupling analysis using the singularity expansion method," *IEEE Trans. Electromag. Compat.*, vol. 36, pp. 358–364, Nov. 1994.

[25] A. G. Tijhuis and H. Blok, "SEM approach to the transient scattering by an inhomogeneous, lossy dielectric slab; Part 1: The homogeneous case," *Wave Motion*, vol. 6, pp. 61–78, 1984.



**George W. Hanson** (S'85–M'91–SM'98) was born in Glen Ridge, NJ, in 1963. He received the B.S.E.E. degree from Lehigh University, Bethlehem, PA, the M.S.E.E. degree from Southern Methodist University, Dallas, TX, and the Ph.D. degree from Michigan State University (MSU), East Lansing, in 1986, 1988, and 1991, respectively.

From 1986 to 1988, he was a development engineer with General Dynamics, Fort Worth, TX, where he worked on radar simulators. From 1988 to 1991, he was a Research and Teaching Assistant with the Department of Electrical Engineering, MSU. He is currently Associate Professor of electrical engineering and computer science at the University of Wisconsin, Milwaukee. His research interests include electromagnetic wave phenomena in layered media and microwave characterization of materials.

Dr. Hanson is a member of URSI Commission B, Sigma Xi, and Eta Kappa Nu.

**Alexander B. Yakovlev** (S'94–M'97–SM'01) was born on June 5, 1964 in the Ukraine. He received the Ph.D. degree in radiophysics from the Institute of Radiophysics and Electronics, National Academy of Sciences, Kiev, Ukraine, in 1992, and the Ph.D. degree in electrical engineering from the University of Wisconsin, Milwaukee, in 1997.

From 1992 to 1994, he was an Assistant Professor with the Department of Radiophysics, Dniepropetrovsk State University, Dniepropetrovsk, Ukraine. From 1994 to 1997, he was a Research and Teaching Assistant with the Department of Electrical Engineering and Computer Science, University of Wisconsin, Milwaukee. From 1997 to 1998, he was an R&D Engineer with Ansoft Corporation/Compact Software Division, Paterson, NJ, and with Ansoft Corporation, Pittsburgh, PA. From 1998 to 2000, he was a Postdoctoral Research Associate with the Electrical and Computer Engineering Department, North Carolina State University, Raleigh. In summer 2000, he joined the Department of Electrical Engineering, The University of Mississippi, University, as an Assistant Professor. His research interests include mathematical methods in applied electromagnetics, modeling of high-frequency interconnection structures and amplifier arrays for spatial and quasioptical power combining, integrated-circuit elements and devices, theory of leaky waves, and singularity theory.

Dr. Yakovlev received the Young Scientist Award presented at the 1992 URSI International Symposium on Electromagnetic Theory, Sydney, Australia, and the Young Scientist Award at the 1996 International Symposium on Antennas and Propagation, Chiba, Japan. He is a member of URSI Commission B.

**Jin Hao** was born in Yuci, Shanxi, China, in 1962. He received the B.Sc. and M.Sc. degrees from Sichuan University, Chengdu, Sichuan, China, in 1985 and 1988, respectively.

From 1988 to 1999, he was an Assistant Lecturer, Lecturer, Associate Professor, and Professor with Taiyuan University of Technology, Taiyuan, Shanxi. Since October 1999, he has been with the Department of Electrical Engineering and Computer Science, University of Wisconsin, Milwaukee, as a visiting scientist. His interests are in the field of electromagnetic theory and antennas.